SPECTRAL BIASES IN BRECCIATED METEORITES: WHAT ARE THEY HIDING? C. D. Schultz[1], R. E. Milliken[1], J. S. Boesenberg[1], and I. Kerraouch[2], [1]Brown University, Providence, Rhode Island, 02912, [2]Institut für Planetologie, University of Münster, Wilhelm-Klemm, Münster, Germany (cody_schultz@brown.edu).

Introduction: Telescopic and spacecraft spectral reflectance measurements of asteroids represent integrations over large areas that can be physically complex and compositionally diverse, as recently highlighted by the results of the Hayabusa2 and OSIRIS-REx missions [e.g., 1, 2]. In order to identify potential biases and better interpret composition (and inferred processes) from such data, it is important to understand how spectra are influenced by small-scale compositional diversity.

These issues may be particularly important for dark and mineralogically complex primitive bodies. Such objects are the presumed source of carbonaceous chondrites, which have been shown to exhibit brecciation at a range of spatial scales [e.g., 3, 4]. Though the diversity of spectral signatures *between* groups of meteorites has been well studied, there remain many questions regarding the diversity of spectral signatures *within* a single chondrite, [e.g., 5,6]. Do different lithologies in brecciated C chondrites have distinct spectral signatures? If so, what factors drive those spectral differences? Are 'bulk' (large spot size) reflectance spectra of brecciated samples biased towards certain lithologies or phases, or are they simply a weighted average of the different lithologies? What do these relationships imply for how we should (or should not) use reflectance spectra of asteroids to infer bulk composition and/or geological processes (e.g., degree of aqueous alteration)?

This study focuses on these questions by comparing detailed spectral and elemental maps for select C chondrites. By integrating these spatially resolved data, we assess and quantify how different components contribute to bulk spectral properties, which in turn can improve interpretations of remotely sensed asteroids.

Methods: We performed a coordinated spectral and petrographic investigation of four sections of the Aguas Zarcas meteorite representing at least three distinct lithologies. Quantitative elemental maps with a spatial resolution of 5 µm were acquired using a Cameca SX-100 electron microprobe. Rasterized IR (~1.6 – 16 µm) spectral reflectance maps were acquired using a Bruker LUMOS microscope FTIR at a spatial resolution of 70–140 µm. 'Bulk' IR spectra with a spatial resolution on the order of the samples themselves (several millimeters) were acquired at the NASA RELAB facility using a Nicolet NEXUS 870 FTIR.

Results: Figure 1 presents an example FeMgSi RGB map of the PL19149 section of the Aguas Zarcas (AZ) meteorite [7,8]. This subsection of AZ exhibits two previously recognized lithologies referred to here as Lithology 1 (a C1/2 lithology [7, 8]) and Lithology 2 (a CM-like lithology [7,8]). The former contains abundant matrix composed of at least two compositions of phyllosilicate, an Mg-rich serpentine-like variety and an Fe-rich variety consistent with tochilinite-cronstedtite intergrowths (TCIs). Minor amounts of sulfide are present along with relic grains of forsteritic olivine. In the framework of [9], this lithology was found to have a petrologic subtype of 2.2. The CM-like lithology exhibits a somewhat more complicated mineralogy with clasts of forsteritic olivine, Al-rich pyroxene, and other lithic phases more abundant than in Lithology 1. The matrix is also more enriched in Fe and S and exhibits heterogeneity in major element compositions. These characteristics are consistent with a less altered, higher petrologic subtype compared with Lithology 1.

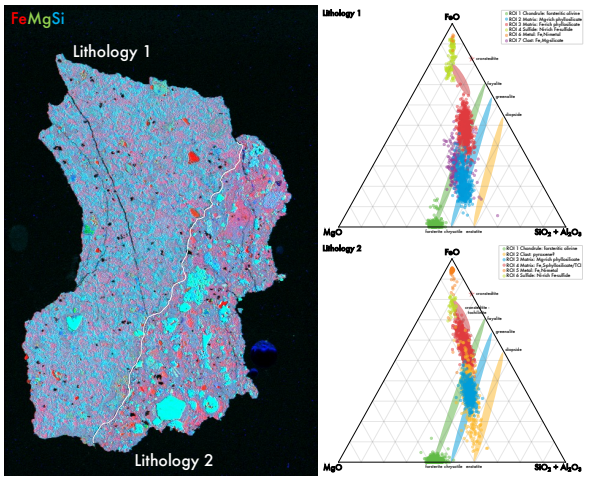

Figure 1: An FeO-MgO-SiO_2 RGB map of the Aguas Zarcas pl19149 section (left) and a FeO-MgO-SiO_2+Al_2O_3 ternary diagram describing the major components of each Lithology 1 and Lithology 2 (right).

Spectral endmembers were initially identified from the µFTIR reflectance maps using K-means clustering. Most spectral endmembers identified through this method represent mixtures of multiple phases within the field of view for each measurement. Elemental maps (e.g., Fig. 1) were used to determine how distinct spectral endmembers relate to different phases throughout each sample. Example spectral endmembers for the AZ section described above are shown in Figure 2, alongside the average spectrum calculated for each lithology and the independently measured 'bulk' FTIR spectrum. Once identified, the endmembers were used to create spectral abundance maps (Fig. 2) by modeling the mid-IR (MIR) spectral range of each map pixel as a linear

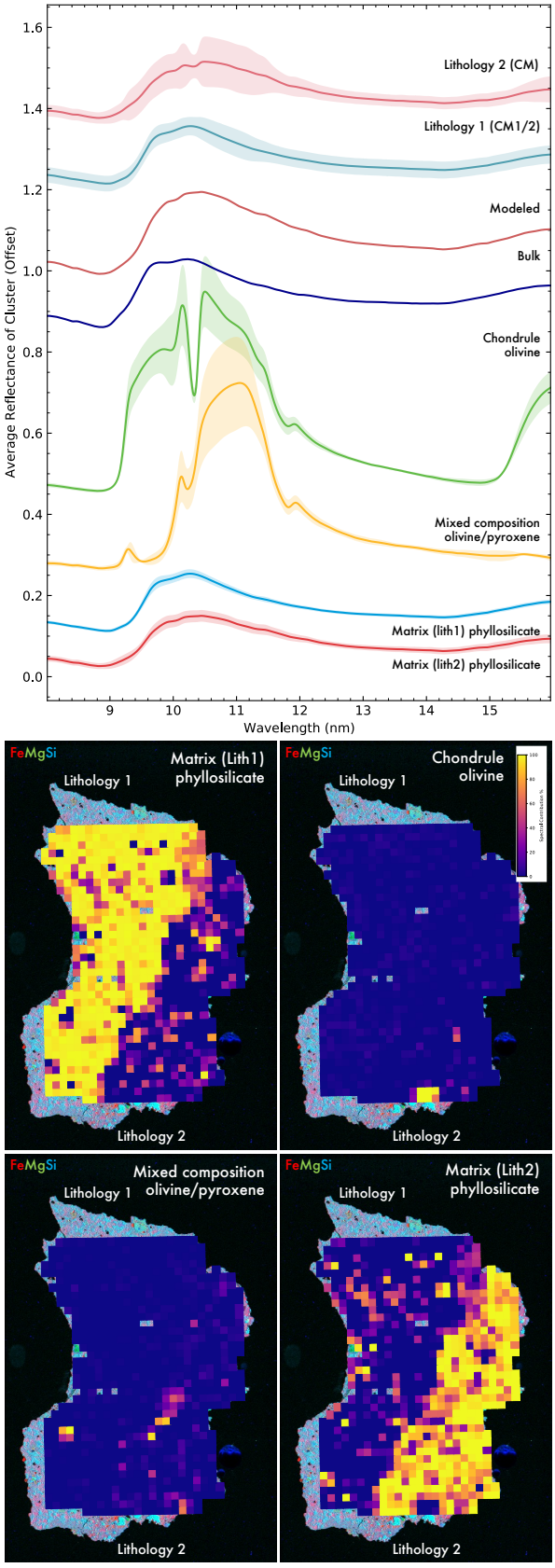

Figure 2: MIR spectra of the four distinct spectral endmembers, the bulk spectrum, the modeled bulk spectrum, and representative spectra of the two main lithologies (top). (Bottom) shows the estimated spectral contribution of each endmember for pixel-level modeling.

combination and solving for the weighting coefficients. Integrating the weighted contribution for each pixel within the spectral map yields a quantitative estimate of the total spectral contribution of each endmember to the bulk spectrum. Endmember spectra are then weighted by this total contribution and summed to produce a forward model of the bulk spectrum for comparison with the actual bulk FTIR spectrum. Independently, the bulk spectrum is modeled via linear least squares to determine the weighting coefficients for each endmember that yields the best spectral fit.

Discussion: Pixel-level modeling produced accurate spectral fits and endmembers were spatially correlated with phases observed in EPMA maps (Figure 2). In contrast, the forward model of the bulk spectrum produced by the µFTIR fit results shows only moderate agreement with the overall shape of the actual bulk FTIR spectrum, and shapes/positions of individual features are poorly matched. The pixel-level spectral fits suggest a 95.69 vol.% total phyllosilicate (both endmembers), with the remainder being pure and mixed composition olivine. In contrast, the actual bulk spectrum can be modeled quite accurately using only the two phyllosilicate endmembers and no contribution of mafic silicates. A similar approach was conducted for the 3 µm region and results will be presented.

Importantly, the µFTIR maps reveal that the two lithologies do exhibit distinct spectral features (Fig. 2), and these differences are likely linked to the differences in the bulk composition of the matrix in these lithologies as observed in the EPMA maps (Fig. 1). Qualitatively, the bulk spectrum appears to be dominated by the representative spectrum of Lithology 1 (C1/2). If similar trends are observed in other brecciated C chondrites it may indicate a tendency for near/mid-IR spectra to overrepresent products of aqueous alteration at the expense of olivine/pyroxene, masking diversity of primitive asteroids.

Acknowledgements: We would like to express our sincere gratitude to Imene Kerraouch, Michael Zolensky, and Philipp Heck for loaning us these intriguing samples.

References: [1] Lauretta et al., (2019) *Nature*, 568. [2] Jawin et al., (2022) *Icarus*, 381. [3] Bischoff et al. (2006) *Meteorites and the Early Solar System II*. [4] Lentfort et al. (2021) *Meteor. & Planet. Sci., 56,* Nr 1. [5] Hamilton et al., (2021) *Nat. Astron,* 5. [6] Schultz et al., (*in press*) *Meteor. & Planet. Sci*. [7] Kerraouch et al. (2021) *Meteor. & Planet. Sci., 56,* Nr 2. [8] Kerraouch et al. (2022) *Geochimca et Cosmochimica Act, 334*. [9] Rubin et al. (2007) *Geochimca et Cosmochimica Act, 71*.